Imperial College London

PLAN OF INVESTIGATION

IMPERIAL COLLEGE LONDON

DEPARTMENT OF EARTH SCIENCE AND ENGINEERING

Modelling the Effects of Projectile Impact on Laminated Window Glass

Supervisors:
John-Paul Latham, Jiansheng Xiang, Ado Farsi

Student:
Michael Trapp

Date: June 27, 2019

1 Introduction

Deliberate acts of terrorism, criminal activity and malicious behaviour pose significant threat to buildings and infrastructure. A recent state-of the arts review by EU decision makers revealed that current building guidelines tend to not take these threats into account. Appropriate regulations and guidelines require new experimental and numerical testing methods to accurately quantify the resilience of building elements against explosions events.

The AMCG at Imperial College London recently developed a novel coupled dynamic gas/solid FEMDEM code, which is proposed to realistically simulate the shock wave impact on secondary laminated glass. In this paper, the code is provisionally applied to simulate 2D and 3D projectile impact on a single laminate. For verification, the results from each simulation are analysed and compared to experimental data from the literature.

2 Physics Theory

2.1 Laminated Glass Model

Laminated glass is a sandwich structure consisting of two brittle glass plies and an adhered visco-elastic polymer inter-layer (or inter-face) in between. An optional back layer improves structural stability and additional energy absorption [1, 2]. The back layer traditionally consists of polycarbonate (PC) [2, 3]. Secondary laminated glass consists of two such laminates, separated by a layer of air.

Advantageous properties of laminated glass include a relatively high penetration resistance [4], low weight [5] and the adherence of fractured glass fragments to the structure to reduce the risk of injuries[4, 6, 7, 8]. Breakage of the inner ply significantly reduces strength and facilitates a full collapse of the glass [7].

The exact prediction of crack initiation and propagation poses a significant challenge and requires ongoing research effort. Local stress intensification is provided by pre-existing micro-structural material flaws (so-called inhomogeneities or discontinuities) such as micro-cracks and voids [9]. Application of fracture stress σ_{f} causes these flaws to grow in size. [7, 10].

Many fracture models have been proposed. This paper uses the combined single and smeared crack model approach [11, 12]. According to the model, increasing stress leads to strain-hardening, followed by strain-softening. Strain-hardening can be modelled with continuum constitutive laws, as failure only occurs in the strain-softening part [13]. The constitutive law for the strain-hardening part is given by

$$\tau = c + \sigma \tan\phi \,, \tag{1}$$

with shear stress τ, normal stress σ, cohesion c and internal friction angle ϕ. The stresses σ and τ correspond to normal and shear displacements δ_{n} and δ_{s} and tensile

and shear strengths f_t and f_s. The material strengths are defined as the maximum strength in the stress-displacement diagram (fig. 1), with maximum elastic displacement δ_p and critical displacement δ_s.

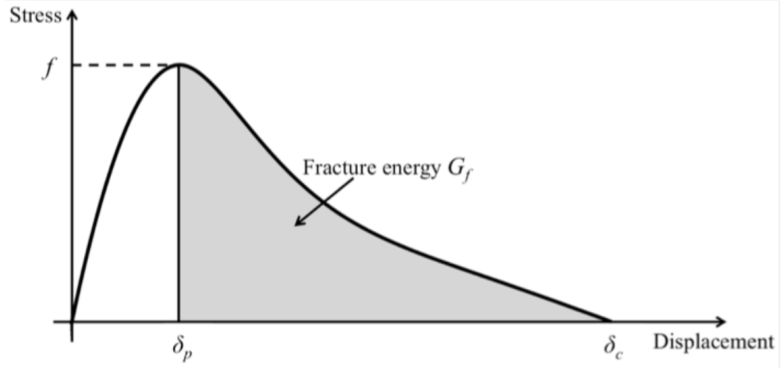

Figure 1: Stress-Displacement Curve. [12]

The fracturing in the strain-softening part is modelled using joint elements which are generated between two neighbouring shell elements. More comprehensive realisations of the model are carried out by Munjiza et al [14], Lei et al [15] and Chen and Chang [16].

2.2 Inter-layer Model

The task of the inter-layer is the absorption of impact energy and the maintenance of adhesion to the plies [5]. Inter-layer materials include polymers such as traditional polyvinyl butyral (PVB), thermoplastic polyurethane (TPU), and most recently SentryGlas®Plus (SGP) [17, 18].

Polymers are commonly modelled as hyper-elastic materials [19, 20]. Work done by stresses onto hyper-elastic materials only depends on the reference state X and the current state x, but not on the load path (fig. 2). Deformation from X to x is described by the deformation gradient [21]

$$F = \frac{\mathrm{d}\varphi}{\mathrm{d}X} \tag{2}$$

with mapping function φ from X to x.
Hyper-elastics are mathematically described by a characteristic strain energy density function W. One of the simplest hyper-elastic models is the Neo-Hookean model [19]. Its characteristic strain energy potential function is given by

$$W = \frac{\mu_0}{2}\left(I_1 - 3\right) - \mu_0 \ln J + \frac{\lambda_0}{2}\ln^2 J\,, \tag{3}$$

with Lamé constants λ_0 and μ_0 from the linearised theory, $J = |F|$ and first invariant $I_1 = C_\mathrm{II}$ with right Cauchy stress tensor [19]

$$C_\mathrm{ij} = F_\mathrm{Ii}\, F_\mathrm{Ij}\,. \tag{4}$$

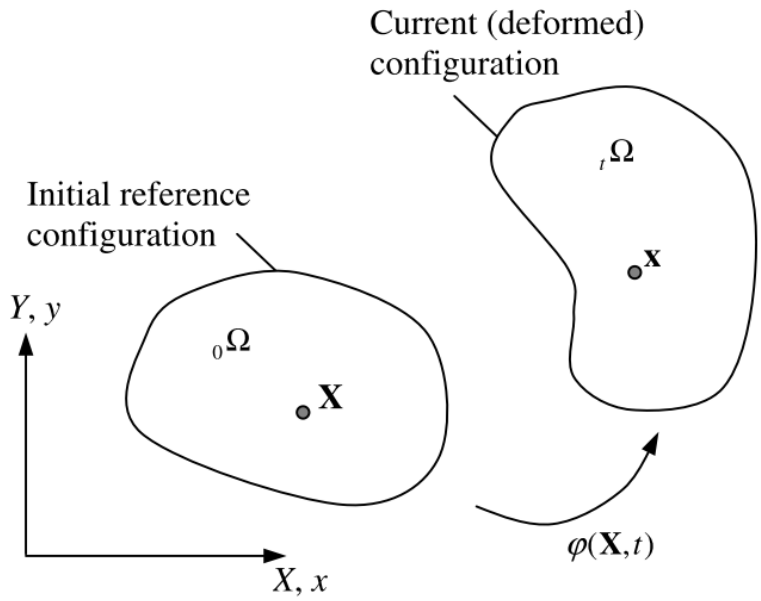

Figure 2: Deformation from reference to current state. [21]

Upper case indices refer to the reference configuration, while lower case indices refer to the current configuration.

Another common, simple hyper-elastic model is the `Mooney - Rivlin` model [22, 23]. The characteristic strain energy function for the compressible 2-Parameter `Mooney - Rivlin` model [23] is given by

$$W_2 = C_{10}\left(\bar{I}_1 - 1\right) + C_{01}\left(\bar{I}_2 - 1\right) + \frac{1}{d}\left(J - 1\right), \tag{5}$$

where C_{10} and C_{01} are adjustable parameters, $d = 2\,/\,K$ with bulk modulus K and $\bar{I}_1 = J^{-\frac{1}{3}}\,I_1$ and $\bar{I}_2 = J^{-\frac{1}{3}}\,I_2$ are deviatoric invariants [22].

Other hyper-elastic models [22] include a more general polynomial model, `Arruda-Boyce`, `Ogden` and `Yeoh`. For the polynomial model, customized coefficients [24] already exist in the literature, specifically for laminated glass.

Modelling the potential occurrence of fracture needs to be permitted for the inter-layer as well. This necessitates an extension of the smeared single and combined fracture model for the inter-layer.

3 Numerics Theory

3.1 FEMDEM

The combined discrete finite element method `FEMDEM` [4, 11, 13, 14, 16, 18, 25, 26, 27, 28] is able to realistically model the deformation, interaction and fracturing of matrix

bodies. The discrete elements consist of clusters of deformable finite elements. Cracks propagate along common finite element boundaries. Fracturing results in the formation of new discrete elements [13].

Conventional FEMDEM methods are significantly inaccurate, as their applied complex shaped polygons require deformability restriction constraints (so-called locking) to maintain stability of the simulation [12].

Munjiza et al [13] developed the novel 2D FEMDEM code Y. The code is based on the so-called F-bar approach which uses 10-noded quadratic elements to reduce volumetric locking. Xiang et al [29] developed the novel 3D FEMDEM code Solidity, Y3D, which features coupled multi-body interaction [12].

3.2 Governing Equations

The governing equations for the finite element calculations in the FEMDEM method are the equations of motion. The equations are given by

$$M\ddot{x} + \mu\dot{x} + f_{\text{int}} = f_{\text{ext}} = f_{\text{l}} + f_{\text{b}} + f_{\text{c}}\,, \tag{6}$$

with lumped nodal mass matrix M, nodal displacements x, viscosity μ, internal nodal forces f_{int} and external nodal forces f_{ext}. External forces contain consist of external loads f_{l}, bonding forces f_{b} and contact forces f_{c}. Internal forces f_{int} are generated by element deformation. FEMDEM systems solve these equations via explicit time integration using the forward Euler method [15].

3.3 Contact Algorithm

The combination of discrete and finite elements is established via an interaction algorithm [15]. This algorithm consists of contact detection [30] and contact interaction [13]. The contact forces between a contractor and target solid are given by

$$f_c = \int_{\Gamma_{\text{c}}} n\left(\varphi_{\text{c}} - \varphi_{\text{t}}\right)\,\mathrm{d}\Gamma_{\text{c}}\,, \tag{7}$$

with outward unit normal n to penetration boundary Γ_{c}, and potential functions φ_{c} and φ_{t} for contractor and target. The contractor applies to the target a normal contact force

$$f_n = -n\int_0^{L_{\text{p}}} p\varphi(l)\mathrm{d}l\,, \tag{8}$$

with penetration length L_{p}, potential function φ along the target edge and penalty term p. It also applies a tangential friction force

$$f_{\text{t}} = \mu_{\text{mob}}\|f_{\text{n}}\|\frac{v_{\text{r}}}{\|v_{\text{r}}\|}\,, \tag{9}$$

with relative velocity v_{r} at the Gauss point and mobilised friction coefficient μ_{mob} which varies during the shearing process. A more detailed explanation is given by Lei et al [15].

3.4 Joint Constitutive Model

The joint constitutive model [12] introduces empirical micro-scale roughness effects to account for dilation and normal stiffness on stressed new and preexisting fracture surfaces.

A more detailed explanation is given by Lei et al [15] and Chen and Chan [16].

4 Numerical Model Approach

4.1 Setup

A 2D input Y file is generated using the pre-processor GID [31]. The geometry could also be imported from common CAD software such as AutoCAD. The input file contains the model including the geometry, constraints, materials, as well as the simulation parameters. The high performance computing (HPC) system at Imperial College London is applied to generate time series images for the simulation. The series is analysed using the post-processing software Hyperview [32]. For the 3D simulation setup, which is is not considered for now, a similar approach will be applied.

4.2 Parameters

Figure 3: 2D geometry of the laminated glass structure and projectile [16]

Fig. 3 illustrates the preliminary 2D geometric setup. The figure shows the initial state of the spherical projectile (yellow) immediately before impact on the laminated glass (impactor glass plies in blue, inner glass ply in red, inter-layer in green). The glass is fixed via a support system (brown). The support structure is not modelled for now and is replaced with no-velocity boundary conditions acting on the sides of the glass plies.

In real-world applications, the dimensions of the inter-layer are smaller than the dimensions of the glass plies. Therefore, a translational degree of freedom in y-direction exists for the inter-layer. This effect will also need to be considered in this paper.

Critical flaws, which cause complete structural failure, are usually found on the cut and machined glass edges [10]. Based on this consideration, the boundary structure layout requires special care. A project task remains to determine a realistic boundary structure to be applied.

The majority of modelling parameters are adduced from the literature. A provisional list of material parameters is given in appendix A. A provisional list of input file simulation parameters is provided in appendix B.

Modifications to this preliminary geometric setup will include changes to the shape of the projectile, as well as changes to the thickness of the layers. A potential consideration is to model the projectile as firearm ammunition instead of a circle (or sphere). A symmetry boundary condition may be applicable and only half of the laminate may need to be modeled.

The dimensions of the glass plate is set to $2000\,\mathrm{mm} \times 2000\,\mathrm{mm}$ in order to avoid anisotropic effects. The thickness of the glass plies is set to $2\,\mathrm{mm}$ and $0.76\,\mathrm{mm}$ for the inter-layer. For now, a PVB material is chosen for the inter-layer. Many models in the literature use similar dimensions, e.g. [14].

The preliminary mesh for all bodies consists of triangular elements. For the 3D model, tetrahedral elements [16] are to be considered. The preliminary element size is $1\,\mathrm{mm}$. Necessary modifications include reducing the number of elements for the projectile, as it is not of interest for the analysis and increasing the element size for far-field mesh elements for the plies and inter-layer. Potentially, differently shaped elements are more optimal for the results. The glass and inter-layers need to consist of several element layers to enable a more precise analysis.

The radius of the steel sphere (or circle) is set to $2.5\,\mathrm{mm}$. The volume of the spherical projectile is given by

$$V = \frac{4\pi}{3} r^3 = \frac{4\pi}{3} \left(2.5\,\mathrm{mm}\right)^3 \approx 65.4\,\mathrm{mm}^3\,. \tag{10}$$

The time step [33] is set accordingly to

$$\Delta t = \sqrt{\frac{V^{1}\,\rho^{2}}{\text{penalty number}}} = \sqrt{\frac{65.4 \cdot 7.8 \cdot 10^3}{4 \cdot 10^{11}}} \approx 1 \cdot 10^{-6}\mathrm{s} \tag{11}$$

To simulate real time $t = 2\,\mathrm{s}$, the maximum number of time steps required [33] is given by

$$n_\mathrm{t} = \frac{t}{\Delta t} = \frac{2\,\mathrm{s}}{10^{-6}\,\mathrm{s}} = 2 \cdot 10^6 \tag{12}$$

4.3 Verification

Numerical simulations need to be verified using data from physical experiments in order to draw conclusions on the degree of accuracy of the numerical model.

Physical experiments involving the breakage of glass by projectiles or shock blasts require special safety arrangements. Air blast impact experiments are being conducted outdoors by service company Jabisupra [34] in cooperation with Imperial College London. The company is active in the field of envelope security and specialises in protecting infrastructure from certain threats. The data from Jabisupra is not expected to

[1] volume $\left(\mathrm{in}\,\mathrm{mm}^3\right)$ of the smallest element, without units
[2] density $\left(\mathrm{in}\,\mathrm{kg/m}^3\right)$ of the material of the smallest element, without units

be ready and applicable for this project. Many other researchers have already conducted impact experiments in the past. A majority of the findings from these experiments are likely to be applicable to verify the model for this project.

Dynamic impact on laminated glass comprises hard and soft body impact [35]. Hard body impact such as ballistic impact [2] causes minimal deformation to the projectile, while soft body impact such as bird impact [35] causes the projectile to undergo extensive deformation.

Relevant parameters of the impact projectile include the normal velocity [5, 36, 37, 38], the mass [37, 38], the angle [36, 37, 38], the shape [38] and the size [5]. Relevant parameters for the outer glass ply include its dimensions [18], its mass, the support conditions [18] and the make-up [18]. For the inter-layer, the material [3, 17, 18], thickness [8, 18, 37] and temperature [17, 39] are relevant.

Low velocity ($\approx 20\,\mathrm{m/s}$) hard impact experiments include the use of projectiles in form of road construction chippings [36], ballistics [3], drop-down weights [18, 30, 40], aluminum projectiles [40] and steel balls [7, 18, 41]. High velocity (around $180\,\mathrm{m/s}$) soft impact experiments include the use of silicon rubber projectiles [35] and gas guns [17].

Wang et al [18] found that the panel size had an inferior effect on the breakage resistance [18]. Similarly, Monteleone et al [3] found that only a local area of the ply around the impact absorbed the impact energy for high velocities.

Karunarathna [37] found that impact velocity and plate thickness contributed significantly towards the impact resistance, compared to impact mass and inter-layer thickness. Wang et al [18] found an increased inter-layer thickness to have a negative effect on energy absorption. Liu et al [42] established that the inter-layer thickness did not contribute towards energy absorption. Behr and Kremer [41] found an increased inter-layer thickness to better protect the inner ply. Kim et al [43] numerically optimised the PVB inter-layer constitution to prevent all damage to the inner glass ply.

Liu et al [42] numerically investigated the optimisability of the inter-layer in terms of energy absorption by simulating the impact of a human head. Zhang et al [39] investigated the influence of temperature on the inter-layer and found that a hybrid TPU/SGP/TPU inter-layer performed best over the entire range of tested temperatures.

5 Hypothesis

The software Solidity is expected to realistically predict and quantify the solid-solid interaction, deformation and fracturing behavior of the laminated window glass upon impact with the projectile. Experimental data from previous research is adduced to further verify this hypothesis.

6 Milestones

due 28 June 2019

1. Compose Plan of Investigation (01-28 June)
2. Review of Current Theory (01-21 June)
3. Software Setup (21-28 June)
4. Specification of Testing Procedures (21-28 June)
5. First Prototype Programme (21-28 June)

due 30 August 2019

6. 2D Simulations (28 June - 12 July)
7. 3D Simulations (12 July - 09 August)
8. Validation/Verification of Results (09 August - 30 August)
9. Outline of Report (28 June - 30 August)
10. Final Draft of Report (01 June - 30 August)

due early-mid September

11. oral presentation

References

[1] L. Biolzi, S. Cattaneo, and G. Rosati. “Progressive damage and fracture of laminated glass beams”. In: *Construction and Building Materials* 24.4 (2010), pp. 577–584. ISSN: 09500618. DOI: 10.1016/j.conbuildmat.2009.09.007 (cit. on p. 2).

[2] X. Brajer, F. Hild, and S. Roux. “On the dynamic fragmentation of glass: A meso-damage model”. In: *International Journal of Fracture* 163.1-2 (May 2010), pp. 121–131. ISSN: 03769429. DOI: 10.1007/s10704-009-9421-9 (cit. on pp. 2, 8).

[3] L. Monteleone, R. Steindler, and G. Kajon. “Monitored ballistic tests on shock-proof sandwich glasses in different conditions”. In: *Experimental Techniques* 28.5 (2004), pp. 28–32. ISSN: 07328818. DOI: 10.1111/j.1747-1567.2004.tb00183.x (cit. on pp. 2, 8).

[4] W. Xu and M. Zang. “Four-point combined DE/FE algorithm for brittle fracture analysis of laminated glass”. In: *International Journal of Solids and Structures* 51.10 (May 2014), pp. 1890–1900. ISSN: 00207683. DOI: 10.1016/j.ijsolstr.2014.01.026 (cit. on pp. 2, 4).

[5] C. D. Wu, X. Q. Yan, and L. M. Shen. “A numerical study on dynamic failure of nanomaterial enhanced laminated glass under impact”. In: *IOP Conference Series: Materials Science and Engineering*. Vol. 10. 1. Institute of Physics Publishing, 2014. DOI: 10.1088/1757-899X/10/1/012176 (cit. on pp. 2, 3, 8, 15).

[6] S. Chen, M. Zang, D. Wang, S. Yoshimura, and T. Yamada. *Numerical analysis of impact failure of automotive laminated glass: A review*. Aug. 2017. DOI: 10.1016/j.compositesb.2017.04.007. URL: https://www.sciencedirect.com/science/article/pii/S1359836816328384 (cit. on p. 2).

[7] F. W. Flocker and L. R. Dharani. “Modeling interply debonding in laminated architectural glass subject to low velocity impact”. In: *Structural Engineering and Mechanics* 6.5 (1998), pp. 485–496. ISSN: 12254568. DOI: 10.12989/sem.1998.6.5.485 (cit. on pp. 2, 8).

[8] F. S. Ji, L. R. Dharani, and R. A. Behr. “Damage probability in laminated glass subjected to low velocity small missile impacts”. In: *Journal of Materials Science* 33.19 (1998), pp. 4775–4782. ISSN: 00222461. DOI: 10.1023/A:1004457624817 (cit. on pp. 2, 8).

[9] P. J. G. Schreurs. *Fracture Mechanics*. Eindhoven, Sept. 2012. URL: http://www.mate.tue.nl/~piet/edu/frm/pdf/frmsyl1213.pdf (cit. on p. 2).

[10] J. Pelfrene, S. V. Dam, R. Sevenois, F. Gilabert, and W. v. Paepegem. “Fracture Simulation of Structural Glass by Element Deletion in Explicit FEM”. In: *Challenging Glass 5 Conference on Architectural and Structural Applications of Glass*. Vol. 5. July. 2016, pp. 439–454. ISBN: 9789082526806. DOI: 10.7480/cgc.5.2270. URL: https://www.researchgate.net/publication/304771271%20https://journals.open.tudelft.nl/index.php/cgc/article/view/2270 (cit. on pp. 2, 6).

[11] A. Munjiza, K. R. Andrews, and J. K. White. “Combined single and smeared crack model in combined finite-discrete element analysis”. In: *International Journal for Numerical Methods in Engineering* 44.1 (Jan. 1999), pp. 41–57. ISSN: 00295981. DOI: 10.1002/(SICI)1097-0207(19990110)44:1<41::AID-NME487>3.0.CO;2-A (cit. on pp. 2, 4).

[12] J.-P. Latham, J. Xiang, A. Farsi, C. Joulin, N. Karantzoulis, A. Obeysekara, and P. Yang. *Solidity Website*. 2019. URL: http://solidityproject.com/ (cit. on pp. 2, 3, 5, 6).

[13] A. Munjiza, Z. Lei, V. Divic, and B. Peros. “Fracture and fragmentation of thin shells using the combined finite-discrete element method”. In: *International Journal for Numerical Methods in Engineering* 95.6 (2013), pp. 478–498. ISSN: 1097-0207. DOI: 10.1002/nme.4511. URL: https://doi.org/10.1002/nme.4511 (cit. on pp. 2, 4, 5).

[14] A. Munjiza. *Ante Munjiza - The Combined Finite-Discrete Element Method*. 2004, p. 350. ISBN: 0470841990. DOI: 10.1002/0470020180 (cit. on pp. 3, 4, 7).

[15] Q. Lei, J.-P. Latham, and J. Xiang. “Implementation of an Empirical Joint Constitutive Model into Finite-Discrete Element Analysis of the Geomechanical Behaviour of Fractured Rocks”. In: *Rock Mechanics and Rock Engineering* 49.12 (Dec. 2016), pp. 4799–4816. ISSN: 0723-2632. DOI: 10.1007/s00603-016-1064-3. URL: http://link.springer.com/10.1007/s00603-016-1064-3 (cit. on pp. 3, 5, 6).

[16] X. Chen and A. H. Chan. “Modelling impact fracture and fragmentation of laminated glass using the combined finite-discrete element method”. In: *International Journal of Impact Engineering* 112 (Feb. 2018), pp. 15–29. ISSN: 0734743X. DOI: 10.1016/j.ijimpeng.2017.10.007 (cit. on pp. 3, 4, 6, 7, 15).

[17] I. Mohagheghian, M. N. Charalambides, Y. Wang, L. Jiang, X. Zhang, Y. Yan, A. J. Kinloch, and J. P. Dear. “Effect of the polymer interlayer on the high-velocity soft impact response of laminated glass plates”. In: *International Journal of Impact Engineering* 120 (Oct. 2018), pp. 150–170. ISSN: 0734743X. DOI: 10.1016/j.ijimpeng.2018.06.002 (cit. on pp. 3, 8).

[18] X. e. Wang, J. Yang, Q. Liu, and C. Zhao. “Experimental investigations into SGP laminated glass under low velocity impact”. In: *International Journal of Impact Engineering* 122 (Dec. 2018), pp. 91–108. ISSN: 0734743X. DOI: 10.1016/j.ijimpeng.2018.06.010 (cit. on pp. 3, 4, 8).

[19] M. H. Ghadiri Rad, F. Shahabian, and S. M. Hosseini. “A meshless local Petrov–Galerkin method for nonlinear dynamic analyses of hyper-elastic FG thick hollow cylinder with Rayleigh damping”. In: *Acta Mechanica* 226.5 (May 2015), pp. 1497–1513. ISSN: 0001-5970. DOI: 10.1007/s00707-014-1266-2. URL: http://link.springer.com/10.1007/s00707-014-1266-2 (cit. on p. 3).

[20] N. H. Kim. *Introduction to nonlinear finite element analysis*. 1st ed. Springer, New York, NY, 2015, pp. XIV, 430. ISBN: 9781441917461. DOI: 10.1007/978-1-4419-1746-1. URL: https://www.springer.com/gp/book/9781441917454 (cit. on p. 3).

[21] Y. T. Gu, Q. X. Wang, and K. Y. Lam. “A meshless local Kriging method for large deformation analyses”. In: *Computer Methods in Applied Mechanics and Engineering* 196.9-12 (2007), pp. 1673–1684. ISSN: 00457825. DOI: 10.1016/j.cma.2006.09.017 (cit. on pp. 3, 4).

[22] Abaqus. *Abaqus Analysis User's Guide*. 2013. URL: http://ivt-abaqusdoc.ivt.ntnu.no:2080/v6.14/books/usb/default.htm (cit. on p. 4).

[23] N. Kumar and V. V. Rao. “Hyperelastic Mooney-Rivlin Model : Determination and Physical Interpretation of Material Constants”. In: *MIT International Journal of Mechanical Engineering* 6.1 (2016), pp. 43–46. ISSN: 2230-7680. URL: https://www.mitpublications.org/yellow_images/75618-me-book.43-46.pdf (cit. on p. 4).

[24] M. A. Samieian, D. Cormie, D. Smith, W. Wholey, B. R. Blackman, J. P. Dear, and P. A. Hooper. “On the bonding between glass and PVB in laminated glass”. In: *Engineering Fracture Mechanics* 214.April (2019), pp. 504–519. ISSN: 00137944. DOI: 10.1016/j.engfracmech.2019.04.006. URL: https://doi.org/10.1016/j.engfracmech.2019.04.006 (cit. on p. 4).

[25] A. Munjiza, D. R. Owen, and N. Bicanic. “A combined finite-discrete element method in transient dynamics of fracturing solids”. In: *Engineering Computations* 12.2 (Feb. 1995), pp. 145–174. ISSN: 02644401. DOI: 10.1108/02644409510799532 (cit. on p. 4).

[26] A. A. Munjiza, E. E. Knight, and E. Rougier. *Computational mechanics of discontinua*. Wiley series in computational mechanics. Chichester, West Sussex, U.K.: Wiley, 2012. ISBN: 9780470970805. DOI: 10.1002/9781119971160 (cit. on p. 4).

[27] L. Guo, J. Xiang, J. P. Latham, and B. Izzuddin. “A numerical investigation of mesh sensitivity for a new three-dimensional fracture model within the combined finite-discrete element method”. In: *Engineering Fracture Mechanics* 151 (Jan. 2016), pp. 70–91. ISSN: 00137944. DOI: 10.1016/j.engfracmech.2015.11.006 (cit. on p. 4).

[28] W. Gao and M. Zang. “The simulation of laminated glass beam impact problem by developing fracture model of spherical DEM”. In: *Engineering Analysis with Boundary Elements* 42 (2014), pp. 2–7. ISSN: 09557997. DOI: 10.1016/j.enganabound.2013.11.011 (cit. on p. 4).

[29] J. Xiang, A. Munjiza, and J. P. Latham. “Finite strain, finite rotation quadratic tetrahedral element for the combined finite-discrete element method”. In: *International Journal for Numerical Methods in Engineering* 79.8 (Aug. 2009), pp. 946–978. ISSN: 00295981. DOI: 10.1002/nme.2599 (cit. on p. 5).

[30] S. Chen, M. Zang, and W. Xu. “A three-dimensional computational framework for impact fracture analysis of automotive laminated glass”. In: *Computer Methods in Applied Mechanics and Engineering* 294 (Sept. 2015), pp. 72–99. ISSN: 00457825. DOI: 10.1016/j.cma.2015.06.005. URL: https://www.sciencedirect.com/science/article/pii/S0045782515001978 (cit. on pp. 5, 8, 15).

[31] GID. *GID, The universal, adaptative and user friendly pre and post processing system for computer analysis in science and engineering. Reference Manual*. 2011. URL: http://www.compassis.com/downloads/Manuals/GiD_User_Manual.pdf (cit. on p. 6).

[32] AltairEngineering. *HyperWorks Desktop Release Notes*. 2017. URL: altairhyperworks.com (cit. on p. 6).

[33] A. Farsi and J. Xiang. *DEM Plus*. 2019 (cit. on p. 7).

[34] J. Zucker, J. Brades, A. New, and A. Toon. *Jabisupra Company Website*. 2016. URL: https://www.jabisupra.co.uk/ (cit. on p. 7).

[35] I. Mohagheghian, Y. Wang, J. Zhou, L. Yu, X. Guo, Y. Yan, M. N. Charalambides, and J. P. Dear. "Deformation and damage mechanisms of laminated glass windows subjected to high velocity soft impact". In: *International Journal of Solids and Structures* 109 (Mar. 2017), pp. 46–62. ISSN: 00207683. DOI: 10.1016/j.ijsolstr.2017.01.006. URL: https://www.sciencedirect.com/science/article/pii/S0020768317300082 (cit. on p. 8).

[36] P. Grant, W. Cantwell, H. McKenzie, and P. Corkhill. "The Damage Threshold Of Laminated Glass Structures". In: *International Journal of Impact Engineering* 21.9 (Oct. 1998), pp. 737–746. ISSN: 0734743X. DOI: 10.1016/s0734-743x(98)00027-x (cit. on p. 8).

[37] K. A. D. L. P. Karunarathna. "Low-Velocity Impact Analysis Of Monolithic And Laminated Glass Using Finite Element Method (FEM)". In: March (2013). URL: https://etheses.bham.ac.uk/id/eprint/5067/2/Kuruvita14MPhil.pdf (cit. on p. 8).

[38] U. A. Dar, W. Zhang, and Y. Xu. "FE Analysis of Dynamic Response of Aircraft Windshield against Bird Impact". In: *International Journal of Aerospace Engineering* 2013 (May 2013), pp. 1–12. ISSN: 1687-5966. DOI: 10.1155/2013/171768 (cit. on p. 8).

[39] X. Zhang, I. K. Mohammed, M. Zheng, N. Wu, I. Mohagheghian, G. Zhang, Y. Yan, and J. P. Dear. "Temperature effects on the low velocity impact response of laminated glass with different types of interlayer materials". In: *International Journal of Impact Engineering* 124 (Feb. 2019), pp. 9–22. ISSN: 0734743X. DOI: 10.1016/j.ijimpeng.2018.09.004 (cit. on p. 8).

[40] F. Mili. "Effect of the Impact Velocity on the Dynamic Response of E-Glass/Epoxy Laminated Composites". In: *Arabian Journal for Science and Engineering* 37.2 (Mar. 2012), pp. 413–419. ISSN: 13198025. DOI: 10.1007/s13369-012-0174-9 (cit. on p. 8).

[41] R. A. Behr, P. A. Kremer, L. R. Dharani, F. S. Ji, and N. D. Kaiser. "Dynamic strains in architectural laminated glass subjected to low velocity impacts from small projectiles". In: *Journal of Materials Science* 34.23 (Dec. 1999), pp. 5749–5756. ISSN: 00222461. DOI: 10.1023/A:1004702100357 (cit. on p. 8).

[42] B. Liu, T. Xu, X. Xu, Y. Wang, Y. Sun, and Y. Li. “Energy absorption mechanism of polyvinyl butyral laminated windshield subjected to head impact: Experiment and numerical simulations”. In: *International Journal of Impact Engineering* 90 (Apr. 2016), pp. 26–36. ISSN: 0734743X. DOI: 10.1016/j.ijimpeng.2015.11.010 (cit. on p. 8).

[43] B. H. Kim, K. C. Ahn, and C. W. Lee. “Low Velocity Impact Behaviors of a Laminated Glass”. In: *Smart Science* 2.4 (June 2016), pp. 209–213. DOI: 10.1080/23080477.2014.11665628 (cit. on p. 8).

[44] J. Xu, Y. Li, X. Chen, Y. Yan, D. Ge, M. Zhu, and B. Liu. “Numerical study of PVB laminated windshield cracking upon human head impact”. In: *Computers, Materials and Continua* 18.2 (2010), pp. 183–211. ISSN: 1546-2218. DOI: 10.3970/cmc.2010.018.183.. URL: http://www.techscience.com/doi/10.3970/cmc.2010.018.183.pdf (cit. on p. 15).

[45] A. Vedrtnam and S. J. Pawar. “Laminated plate theories and fracture of laminated glass plate - A review”. In: *Engineering Fracture Mechanics* 186 (2017), pp. 316–330. ISSN: 00137944. DOI: 10.1016/j.engfracmech.2017.10.020 (cit. on p. 15).

[46] M. A. Samieian, D. Cormie, D. Smith, W. Wholey, B. R. Blackman, P. A. Hooper, and J. P. Dear. “Delamination in Blast Resistant Laminated Glass”. In: *21st International Conference on Composite Materials Xi’an, 20-25th August 2017* August (2017), pp. 20–25. DOI: 10.1016/j.ijimpeng.2017.09.001 (cit. on p. 15).

[47] J. Stampfl and O. Koldenik. “The separation of the fracture energy in metamaterials”. In: *International Journal of Fracture* 101 (2000), pp. 321–345. URL: http://info.tuwien.ac.at/stampfl/publikationen/lok_glob.pdf (cit. on p. 15).

[48] M. Y. Zang and S. H. Chen. “Laminated glass”. In: ed. by L. Nicolais and A. Borzacchiello. Second Edi. Guangzhou: Joh Wiley &, 2012. DOI: https://doi.org/10.1002/9781118097298.weoc121 (cit. on p. 15).

[49] J. K. Kuntsche. *Mechanical behaviour of laminated glass under time-dependent and explosion loading*. German. Darmstadt: Springer-Verlag Berlin Heidelberg, 2015, p. 265. ISBN: 978-3-662-48830-0. DOI: 10.1007/978-3-662-48831-7 (cit. on p. 15).

[50] M. Sahin, C. S. Çetinarslan, and H. E. Akata. “Effect of surface roughness on friction coefficients during upsetting processes for different materials”. In: *Materials and Design* 28.2 (2007), pp. 633–640. ISSN: 18734197. DOI: 10.1016/j.matdes.2005.07.019 (cit. on p. 15).

[51] M. Fahlbusch. “Zur Ermittlung der Resttragfähigkeit von Verbundsicherheitsglas am Beispiel eines Glasbogens mit Zugstab”. German. In: (Mar. 2007), pp. 1–123. URL: http://elib.tu-darmstadt.de/diss/000962 (cit. on p. 15).

A Material Parameters

Property	Glass	PVB	Steel Projectile
Density ρ $[\mathrm{kg/m^3}]$	2500 [44]	1100 [44]	7800 [16]
Young's Modulus E $[\mathrm{Pa}]$	7e10 [44]	2.2e2 [45]	2e11 [16]
Poisson's Ratio ν	0.22 [44]	0.49 [30]	0.3 [16]
Mass damping coefficient μ	0	0	0
Elastic penalty term	7e10	2.2e2	2e11
contact penalty	1.4e11	4.4e2	4e11
Mode I energy rate G_{I} $[\mathrm{J/m^2}]$	10 [44]	2.8e3 [46]	1.9e5 [47]
Mode II energy rate G_{II} $[\mathrm{J/m^2}]$	50 [44]		
Mode III energy rate G_{III} $[\mathrm{J/m^2}]$	50 [44]		
Tensile Strength σ $[\mathrm{Pa}]$	6e7 [30]	2e7 [48]	1e7 [5]
Internal friction coefficient	0.1 [30]	0.7 [49]	0.15 [50]
Internal cohesion $[\mathrm{Pa}]$	7e10	2.2e2	2e11
Pore fluid pressure $[\mathrm{Pa}]$	0	0	0
Joint friction coefficient			
Joint roughness coefficient $\mathtt{JRC}_0$ [3]			
Joint compressive strength $\mathtt{JCS}_0$ [3]			
Joint sample size $[\mathrm{m}]$			
Interface friction	0.1 [30]	0.62 [51]	0.44 [51]
2D Problems	plane stress		

Table 1: List of preliminary Y2 input material parameter values.

[3] at laboratory conditions

B Simulation Parameters

Parameter	Value
Maximum number of timesteps	2e6
Current number of timesteps	0
Restart file saving frequency	1e2
Gravity in X Direction (m/s2)	0
Gravity in Y Direction (m/s2)	0
Gravity in Z Direction (m/s2)	-9.8
Timestep (s)	1e-6
Output frequency	10
Current number of iterations	0
Gravity setting stage (s)	0
Load ramping stage (s)	0
Maximum dimension (m)	10
Maximum force (N)	1e6
Maximum velocity (m/s)	100
Maximum stress (Pa)	1e8
Maximum displacement (m)	0.1
Minimum joint aperture (m)	1e-7
Maximum contacting couples	1e7
Accuracy (bit)	32
Joint friction model	Coulomb
Initial aperture correlation	roughness

Table 2: List of preliminary Y2D input simulation parameter values.